Catalysis
Science & Technology

RSC Publishing

PAPER

View Article Online
View Journal | View Issue

Cite this: *Catal. Sci. Technol.*, 2013, **3**, 2425

Selective oxidation of benzyl alcohol using *in situ* generated H_2O_2 over hierarchical Au–Pd titanium silicalite catalysts†

Inés Moreno,[ab] Nicholas F. Dummer,[a] Jennifer K. Edwards,[a] Mosaed Alhumaimess,[a] Meenakshisundaram Sankar,[a] Raul Sanz,[b] Patricia Pizarro,[b] David P. Serrano[bc] and Graham J. Hutchings*[a]

Received 12th July 2013,
Accepted 15th July 2013

DOI: 10.1039/c3cy00493g

www.rsc.org/catalysis

Benzyl alcohol was oxidized by an ''*in situ* generated'' hydrogen peroxy species, formed from a dilute mixture of hydrogen and oxygen, under mild conditions at a high rate over gold, palladium and gold–palladium nanoparticles supported on hierarchical titanium silicate materials. Hierarchical TS-1 supports were obtained from the crystallization of silanized protozeolitic units, being characterized by having a secondary porous system within supermicro/mesopore range and an enhanced surface area over a standard reference TS-1 material. The presence of the secondary porosity not only improves the accessibility to the active sites of the relatively large reactant molecules but also enhances the metal dispersion, leading to an improved catalytic performance for alcohol oxidation. The catalytic activity of metal loaded hierarchical TS-1 materials was found to be higher in reactions conducted in the presence of diluted hydrogen and oxygen, resulting in a 5-fold increase in the yield of benzaldehyde at 30 °C with an AuPd catalyst with secondary porosity. The improvement in rate observed is due to the oxidizing efficacy of *in situ* generated hydroperoxy species as compared to molecular oxygen alone as the terminal oxidant.

Introduction

Titanium silicate (TS-1)[1] materials have emerged as effective catalysts for the oxidation of various substrates using environmentally benign oxidants, for example hydrogen peroxide.[2–4] TS-1 possesses an MFI structure which consists of three dimensional pore system of 10 ring channels arranged sinusoidally (5.1 × 5.5 Å) with an intersecting straight 10-ring channel (5.3 × 5.6 Å).[5] As with other such zeotype materials, which possess microporosity, they are limited in their application with bulky reactant molecules. The synthesis of hierarchical zeolite materials facilitates increased reactant diffusion towards the active sites within the pore structure.[6,7] Preparation of such materials covers a wide range of strategies detailed in a review by van Donk *et al.*[8]

Hierarchical TS-1 has been obtained with hard-templates based on porous carbon[9,10] and soft templates such as surfactants or organosilane molecules.[11,12] Recently, it has been reported the preparation of hierarchical TS-1 materials from the crystallization of silanized protozeolitic units.[13,14] In this strategy, an organosilane compound is added to a solution of protozeolitic units, formed previously by a precrystallization step. These organosilanes anchor onto the external surface and thereby partially block the aggregative growth during the final hydrothermal treatment. After this crystallization step, a secondary porosity, in addition to the typical zeolite micropores, is formed when the organosilane compound is removed by calcination. These materials have been evaluated in alkene epoxidation, with both H_2O_2 and tertiary-butyl hydroperoxide (TBHP). The use of alkyl peroxides, typically with bulky structures, is generally ineffective with TS-1 due to the restrictive microporous structure.[15,16] Enhancements in product yield were achieved with those materials with secondary porosity, where the increased surface area was related to an improved turnover frequency.[14]

Selective oxidation with TS-1 is generally carried out with hydrogen peroxide as an oxidant and is successful in a large number of applications.[15,17–21] Typically, however, hydrogen peroxide is used as a stoichiometric oxidant which is considered expensive. Heterogeneous gold catalysts represent a promising

[a] *Cardiff Catalysis Institute, School of Chemistry, Cardiff University, Cardiff, CF10 3AT, UK. E-mail: hutch@cardiff.ac.uk*
[b] *Department of Chemical and Energy Technology, ESCET, Rey Juan Carlos University, c/ Tulipán s/n, Móstoles, 28933, Madrid, Spain*
[c] *IMDEA Energy Institute, Avda. Ramón de la Sagra, 3, Móstoles, 28935, Madrid, Spain*

† Electronic supplementary information (ESI) available. See DOI: 10.1039/c3cy00493g

alternative to the use of stoichiometric radical initiators, where oxygen can be activated and incorporated in the final product.[22] Furthermore, *in situ* generation of hydroperoxy species with subsequent reaction to an oxygenated target represents a desirable, lower cost route. The recent review by Della Pina *et al.*[23] highlighted advances in selective oxidation over gold catalysts with emphasis on the emerging industrial applications. Haruta *et al.*[24] have demonstrated low temperature epoxidation of propene at the gas–solid interface. This process requires the use of sacrificial hydrogen to form a surface peroxy species *in situ*, which is able to complete the formation of propene oxide with high specificity. The catalyst used for this process involved gold nanoparticles supported on TiO_2 and improvements in activity have been obtained more recently with supports including TS-1, Ti-MCM-41 and Ti-MCM-48.[25–30]

Selective oxidation in three phase systems with *in situ* generated hydroperoxy species is an emerging topic.[31–36] However, the activity of the catalyst used must be sufficiently high to operate at the temperatures associated with direct hydrogen peroxide production which is low, and typically sub-ambient.[37,38] Thermal decomposition of hydrogen peroxide occurs readily above ambient temperatures and rapidly in the presence of transition metals. The aerobic oxidation of benzyl alcohol to benzaldehyde under mild conditions has been shown to occur with the same catalyst systems as used for direct peroxide synthesis.[38,39] These include supported gold–palladium nano-particles which have a high activity and selectivity to benzaldehyde. Generally, equimolar Au–Pd mixtures are considered to be advantageous as monometallic gold catalysts typically have poor activity. However, increasing the Pd content increases the formation of one of the by-products, toluene, which is undesirable. Attempts with Au–Pd supported on zeolitic materials for the oxidation of cyclohexane with *in situ* peroxy species has shown promise.[32] However, the yields of cyclohexanol were found to be low; *ca.* 2%, more success was obtained with crotyl alcohol oxidation to crotonaldehyde over 2.5% Au–2.5% Pd/TS-1 catalyst with a yield of *ca.* 25% over 4 h at 60 °C.[32] It was concluded that the rate of oxidation should be comparable to the production rate of peroxy species to ensure that the hydrogenation of the substrate (if applicable) is not dominant with Pd containing catalysts.

The use of on-site, small-scale hydrogen peroxide production for a range of applications is desirable with respect to storage and transportation costs of concentrated peroxide (typically 70 wt%). In this paper we report the application of *in situ* generated hydroperoxy species at low concentrations with hierarchical TS-1, prepared from silanized protozeolitic units, as a support to gold and palladium nano-particles for benzyl alcohol oxidation as a model reaction. These TS-1 zeolites, which possess a significant mesoporosity can improve both the accessibility of the reactants to the active sites as well as enhancing the metal dispersion and controlling the metal particle size. For this reason, the production rate of benzaldehyde from the oxidation of benzyl alcohol will be used to evaluate these hierarchical materials as catalysts with dual functionality.

Experimental

Catalyst preparation

TS-1 (XG-REF): sample prepared from amorphous SiO_2–TiO_2 xerogel. The amorphous SiO_2–TiO_2 xerogel used as raw material was synthesized by a sol–gel method comprising two steps according to Serrano *et al.*[40] employing tetra-ethylorthosilicate (TEOS, Alfa) and titanium tetra-butoxide (TNBT, Acros) as silica and titanium sources, respectively, and tetra-propylammonium hydroxide (TPAOH) as gelification agent. The final molar composition of the raw xerogel was as follows: 1.0 SiO_2 : 0.016 TiO_2 : 0.0355 TPAOH. Once the SiO_2–TiO_2 xerogel was obtained, it was impregnated with a 1 M TPAOH aqueous solution employing a TPAOH/xerogel mass ratio of 2.75 and, then, it was crystallized at 170 °C using heating by microwave radiation for 8 h in PTFE vessels under autogenous pressure.

TS-1 (LG-*x*%): samples obtained from liquid gels where *x*% represents the mol% of phenyl amino-propyltrimethoxysilane (silanization agent). These samples were prepared according to a protozeolitic units silanization method reported previously.[13,14,41] First, a synthesis gel with a molar composition of 1.0 SiO_2 : 0.016 TiO_2 : 0.44 TPAOH : 28.5 H_2O was prepared following the original recipe developed by Taramasso *et al.*[1] This solution was pre-crystallized in a reflux system under stirring conditions at 90 °C for 24 h. The silanization agent (phenyl amino-propyltrimethoxysilane, PHAPTMS, Aldrich) was added at the desired loading (5, 8 and 12 mol%) in regard to the total silica content in the gel, the functionalization reaction being carried out under stirring at 90 °C for 6 h. Finally, the crystallization of the TS-1 zeolite was performed by microwave heating at 170 °C for 8 h in PTFE vessels under autogenous pressure. In all cases, the solid products obtained after the crystallization treatment were separated by centrifugation, washed several times with distilled water, dried (16 h, 110 °C) and calcined (in static air conditions 550 °C, 5 h).

Preparation of Au, AuPd and Pd nanoparticles supported on titanium silicates. The impregnation method (IM) was used to prepare a 2.5 wt% Au catalyst, an aqueous solution of $HAuCl_4 \cdot 3H_2O$ (2.5 mL, 2 g in 100 mL distilled water) was added to the support (1 g). The mixture was stirred at 80 °C for 4 h. Then, the paste formed was ground and dried at 110 °C for 16 h. 2.5 wt% Pd/support was prepared following the same procedure using a solution of $PdCl_2$. Bimetallic Au–Pd catalysts, comprising 2.5 wt% of each metal (*i.e.* 1 : 1.85 molar ratio Au : Pd), were prepared using the same procedure with appropriate amounts of $HAuCl_4 \cdot 3H_2O$ and $PdCl_2$. Prior to use, samples were also calcined at 400 °C in static air for 3 h.

The materials 2.5 wt% Au–Pd/support were also prepared using the following deposition precipitation method (denoted DP). For the catalyst, a solution of $HAuCl_4 \cdot 3H_2O$ (2.5 mL, 2 g in 100 ml distilled water) and $PdCl_2$ was diluted with water (50 mL). An aqueous sodium hydroxide solution (0.1 M) was added with stirring until pH = 9 was attained. Then, support (1 g) was added over the previous solution, with continuous stirring. The mixture was heated at 70 °C for 1 h maintaining the pH at 9. The solid was recovered by centrifugation and washed several times with

Table 1 Catalysts used and their preparation method

Catalyst	Metal[a] (wt%)	Preparation method	Support
AX	Au (2.5)	IM	TS-1 (XG-REF)
A12	Au (2.5)	IM	TS-1 (LG-12%)
PX	Pd (2.5)	IM	TS-1 (XG-REF)
P12	Pd (2.5)	IM	TS-1 (LG-12%)
APX	Au–Pd (2.5)	IM	TS-1 (XG-REF)
AP5	Au–Pd (2.5)	IM	TS-1 (LG-5%)
AP8	Au–Pd (2.5)	IM	TS-1 (LG-8%)
AP12	Au–Pd (2.5)	IM	TS-1 (LG-12%)
DAPX	Au–Pd (2.5)	DP	TS-1 (XG-REF)
DAP12	Au–Pd (2.5)	DP	TS-1 (LG-12%)

[a] Per metal, IM = impregnation, DP = deposition precipitation.

distilled water. Finally, the catalyst was dried (110 °C, 16 h) and calcined at 400 °C in static air for 3 hours.

Catalysts used in this study and their preparative routes together with their codes are summarised in Table 1.

Catalyst characterisation

Powder X-Ray Diffraction (XRD) patterns were measured using a Philips X'PERT MPD diffractometer operating with Cu Kα radiation with a step size and time of 0.02° and 10 s, respectively. The coordination of the titanium atoms in the samples, as well as the possible presence of extra-framework TiO_2 phases, was checked by Diffuse Reflectance UV-VIS spectroscopy (DR UV-VIS) under ambient conditions with a Varian Cary-500 spectrophotometer equipped with a diffuse reflectance accessory and using $BaSO_4$ as reference. The spectra were monitored in the range of 200–500 nm. Titanium content of the synthesized samples was estimated by means of inductively coupled plasma atomic emission spectroscopy (ICP-AES) analysis, performed in a Varian Vista AX system. Likewise, the total surface area was estimated according to the BET method by means of argon adsorption–desorption isotherms at 87 K, acquired with a Micrometrics ASAP 2010 instrument. The samples were out-gassed prior to the analysis at 300 °C under vacuum for at least 16 h. The pore size distribution and cumulative volume curves were calculated by applying the NL-DFT model with cylindrical pore geometry. TEM images were obtained in a Philips Technai 20 electron microscope operating at 200 kV and a resolution of 2.7 Å. The samples for TEM were prepared by dispersing the sample powder in acetone and drying a droplet of the suspension onto a carbon-coated copper grid.

Catalyst testing

Reactions using a glass reactor. Catalytic oxidation reactions were performed in a round bottom glass reactor (Colaver, 50 mL) at a constant pressure of oxygen (1.2 barg) and heated in an oil bath. Benzyl alcohol (2 g, 0.0185 mol) and catalyst (0.02 g) were placed in the reactor and the gas present purged with successive charges of oxygen. The reaction mixture was then stirred with a magnetic follower until the desired temperature (120 °C). The reactions were carried out for 4 h. Analysis was carried out using gas chromatography (Varian star 3400 CX) with CP-WAX 52 CB column (25 m length, 0.53 mm O.D. and 0.2 μm film thickness) and a flame ionization detector. Mesitylene was used as internal standard for the calculation of benzyl alcohol conversion and product yields and selectivities are expressed as mol%. The products were characterized by Gas-Chromatography coupled with Mass Spectrometer (GC-MS). Then, the retention times of these samples were compared with that of pure standards injected in GC.

Reactions using a stainless steel reactor. Hydrogen peroxide synthesis and benzyl alcohol oxidation were conducted in a high pressure stainless steel autoclave (50 mL, Parr Instruments), featuring over-head stirring (1200 rpm). Typically reactions were carried out at 2 or 30 °C over 30 min under an atmosphere of either 25% O_2/CO_2 (10.34 bar, 150 psi) or for reactions with *in situ* generated H_2O_2; 5% H_2/CO_2 (28.96 bar, 420 psi) and 25% O_2/CO_2 (10.34 bar, 150 psi). In these high pressure experiments CO_2 was used as the diluent for reasons of safety as with CO_2 the explosive region of the H_2–O_2 mixture is minimized, however, the use of CO_2 has an added benefit of acting as an *in situ* acid stabilizer of the hydrogen peroxide that is formed. The catalyst (10 mg) was added to a mixture of methanol (5.6 g) and water (2.9 g) and the benzyl alcohol (0.25 g, 2.3 mmol) was then added, the vessel was then sealed and stirring commenced. Product analysis was carried out using gas chromatography as above described. H_2O_2 yield was determined by titration of aliquots of the final filtered solution with acidified $Ce(SO_4)_2$ (7×10^{-3} mol L^{-1}). $Ce(SO_4)_2$ solutions were standardized against $(NH_4)_2Fe(SO_4)_2 \cdot 6H_2O$ using ferroin as indicator.

Turn over frequency (TOF) is defined as the total moles of benzaldehyde produced per hour divided by the total moles of metal present in the reaction.

Results and discussion

In this work, hierarchical titanium silicates materials (TS-1), prepared by silanization of protozeolitic units,[13,14] were used as a support for gold and palladium nanocrystals (Au, Pd). For comparison purposes, a microporous conventional TS-1 zeolite prepared from amorphous SiO_2–TiO_2 xerogel was also employed as support.

Catalyst characterization

Parent TS-1 characterization. Fig. 1 shows the XRD patterns of the hierarchical TS-1 materials obtained from silanized protozeolitics units and a conventional TS-1 sample prepared from SiO_2–TiO_2 amorphous xerogel. Diffraction reflections corresponding to the MFI structure are observed for all the samples, denoting that they are highly crystalline. However, reflections for the hierarchical TS-1 obtained from silanized protozeolitic units are broader and less intense than those for the conventional TS-1 reference material (TS-1 (XG-REF)). This is attributed to a reduction in the size of the crystalline domains, due to their hindered growth caused by the silanization agent. Diffused Reflectance (DR) UV-Vis analyses of the samples (Fig. S1, see ESI†) revealed that in all the samples most of the titanium atoms are in the tetrahedral coordination because of the presence of a band around 220 nm. The absence of 330 nm band for all the samples ruled out the presence of extra framework Ti atoms in the materials.

The application of the NL-DFT model over the Ar adsorption–desorption isotherms (87 K) allows the pore size distribution in the micro- and mesopore region to be estimated within the complete micro/mesopore range. Fig. 2 illustrates the cumulative

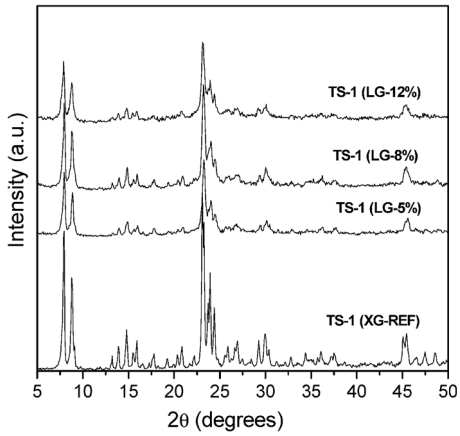

Fig. 1 Powder XRD patterns of calcined TS-1 (XG-REF), TS-1 (LG-5%), TS-1 (LG-8%) and TS-1 (LG-12%) samples.

pore volume and pore size distribution (PSD) curves corresponding to the hierarchical TS-1 zeolites compared to the curves obtained for the reference zeolite. In all cases, a narrow peak with a maximum around 5.5 Å is detected in the PSD curve which agrees with the pore size of the MFI structure. However, in the pore size distribution curves corresponding to the hierarchical samples, an additional adsorption is detected between 10–60 Å, related to the presence of the secondary porosity in the supermicro/mesopore region, caused by the inhibitor growth effect of the silanization agent during the zeolite crystallization. The presence of this secondary porosity not only could increase the mass transport into the zeolite channels but could also improve the incorporation and dispersion of the metal particles onto the zeolitic surface, since they could be located into the secondary porosity while in the conventional microporous zeolite the metal particle are usually concentrated over the zeolitic crystal external surface.[42]

The textural properties of the TS-1 samples were obtained by applying the NL-DFT model from Ar adsorption–desorption isotherms (Table 2). The subscripts ZM and SP make reference to the zeolitic micropores and the secondary porosity, respectively. Hierarchical TS-1 samples prepared from silanized protozeolitic units were found to possess higher BET and secondary porosity surface areas than the reference zeolite. Thus, while for the reference TS-1 sample the latter values were *ca.* 470 $m^2 g^{-1}$ and *ca.* 53 $m^2 g^{-1}$, respectively, such values increased up to 656 $m^2 g^{-1}$ and 400 $m^2 g^{-1}$, respectively, for TS-1 (LG-12%). This increase of the BET surface area, which is exceptionally high when compared to the conventional MFI zeolites, corresponds to the surface area of the secondary porosity. A clear relationship is observed between the amount of silanization agent introduced into the synthesis gel and the modification degree of the hierarchical TS-1 textural properties.

Finally, the morphology of the reference TS-1, TS-1 (XG-REF), and the hierarchical catalyst, TS-1 (LG-8%), were analyzed by TEM microscopy (Fig. 3). It can be observed that reference TS-1 (XG-REF) zeolite is formed by large particles with an average dimension of around 2 μm and regular and well defined edges. On the other hand, TS-1 (LG-8%) consists in slightly large aggregates with dimensions around 150–200 nm and sponge-like morphology. From images taken at higher magnifications it

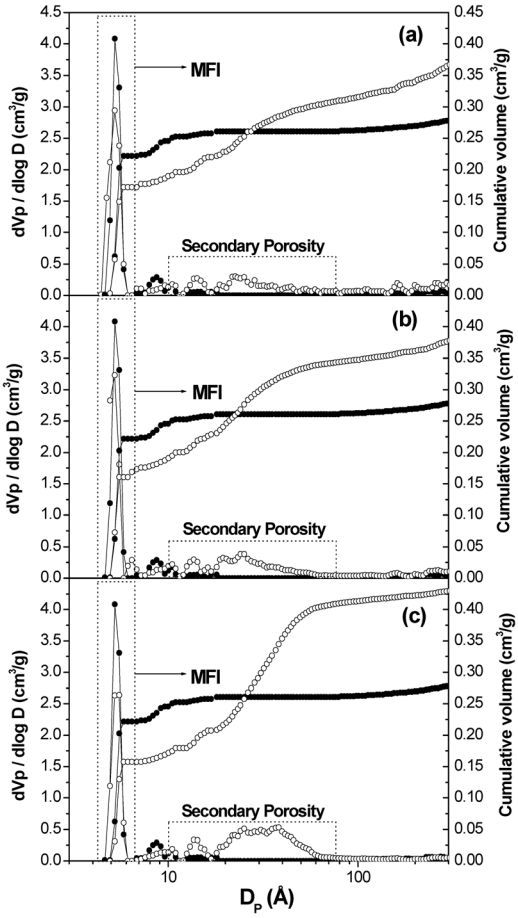

Fig. 2 Cumulative pore curve and pore size distribution for TS-1 (XG-REF) (●) compared to (a) TS-1 (LG-5%) (○), (b) TS-1 (LG-8%) (○) and (c) TS-1 (LG-12%) (○) and estimated by applying NL-DFT method to Ar adsorption isotherms at 87 K.

may be distinguished that these aggregates are formed by ultra-small crystalline domains (nano-units) with dimensions below or around 20–25 nm. The voids existing between these nano-units are related to the secondary porosity caused by the silanization agent. The presence of diffraction fringes in these units indicates their crystalline nature.

AuPd/TS-1 catalysts. Analysis by TEM of the AuPd catalysts supported on TS-1 with and without secondary porosity is displayed in Fig. 4. Two methods of metal disposition were analysed; impregnation (IM) and deposition precipitation (DP). The addition of the metals to the TS-1 material with both methods indicates that the presence of secondary porosity is important with respect to the AuPd particle size. In the case of the conventional TS-1 the AuPd particle size with impregnation are 100–180 nm (mean 133 nm) and 20–30 nm (mean 26 nm) for deposition precipitation. Deposition on the TS-1 materials with secondary porosity decreases the average particle size to *ca.* 2–3 nm (mean 2.2 nm) and 4–8 nm (mean 6.7 nm), respectively. The large size of the AuPd particles on the standard TS-1 deposited by impregnation have been reported before.[43] Typically, this can lead to lower catalytic activity due to the increased proportion of bulk metal. However, according to the model proposed by Haruta *et al.*,[24] which was based on theoretical work by Olivera *et al.*,[44] reactions occur upon a Ti containing surface

Table 2 Ti content and textural properties estimated by applying NL-DFT method to Ar isotherms at 87 K of titanium silicalites

Material	% Ti	Si/Ti (mol)	S_{BET} (m^2 g^{-1})	S_{ZM} (m^2 g^{-1})	S_{SP} (m^2 g^{-1})	V_{ZM} (cm^3 g^{-1})	V_{SP} (cm^3 g^{-1})
TS-1 (XG-REF)	1.32	59.0	469	416	53	0.222	0.075
TS-1 (LG-5%)	0.97	80.3	560	280	280	0.172	0.233
TS-1 (LG-8%)	1.39	56.0	633	263	371	0.161	0.239
TS-1 (LG-12%)	1.37	56.8	656	256	400	0.157	0.281

S_{BET} = surface area by BET method, V = pore volume, ZM = zeolitic micropores, SP = secondary porosity.

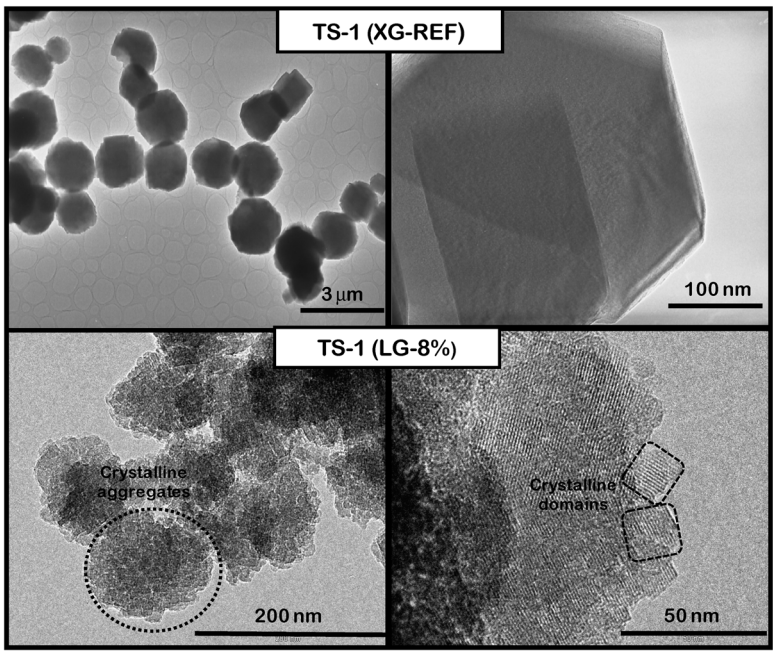

Fig. 3 TEM micrographs of TS-1 (XG-REF) and TS-1 (LG-8%) samples.

where a hydroperoxy species has formed *in situ* on the Au surface and joins the Ti surface activated propene. The large particle size of the AuPd may not be detrimental due to reactions occurring at or near an interfacial surface site, although Haruta reports that a particle size of between 2–4 nm are desirable.

Catalyst testing

The catalysts were investigated for solvent-free benzyl alcohol oxidation at 120 °C under moderate oxygen pressure and the results are illustrated in Table 3. They indicate that the secondary porosity of the hierarchical catalysts; AP5-12, DAP12 and P12 facilitated improved activity compared to standard TS-1 catalysts under these conditions. However, for catalysts AP5 and AP8 similar catalytic activity was observed. In general, the presence of an additional mesoporosity in zeolites improves the reactant and product diffusion leading to a higher conversion. This can be probed by pore size distributions and textural properties of the catalysts (Table 2) compared to the size of the benzyl alcohol molecule (length *ca.* 7.9 Å, width *ca.* 5.3 Å (calculated with Accelrys Materials Studio 6.0; Dmol3 geometry optimisation)). Moreover, it is possible that this secondary porosity enhances the degree of incorporation and dispersion of the metal particles. The respective benzaldehyde production rate and turn-over frequency (TOF) over APX was calculated to be 75 ± 0.5 mol h^{-1} $kg_{cat}{}^{-1}$ and 332 h^{-1} compared to catalyst AP12 with 135 ± 0.5 mol h^{-1} $kg_{cat}{}^{-1}$ and 615 h^{-1}. However, the method of metal deposition and metal choice dominates both the level of conversion and benzaldehyde selectivity despite the obvious reduction in diffusion limitations. The combination of Au–Pd leads to increased catalyst activity, observed previously.[45] When catalysts were prepared with deposition precipitation the selectivity to benzaldehyde is increased relative to those prepared *via* impregnation. Catalyst DAP12 achieved a benzaldehyde production rate of 171 ± 0.5 mol h^{-1} $kg_{cat}{}^{-1}$. Conversely, those prepared by impregnation were more active, however, with an increased amount of the by-product; toluene (Fig. 5). Toluene is formed by the disproportionation of benzyl alcohol to equimolar mixture of benzaldehyde and toluene.[46] Disproportionation is observed in greater amount with impregnation catalysts, which we consider is related to the particle size of the metal nano-particle and potentially the Pd surface (Fig. 4). Such disproportionation of benzyl alcohol to benzaldehyde, toluene and water has been reported previously and occurs at elevated temperatures over Pd only or Pd containing catalysts.[47]

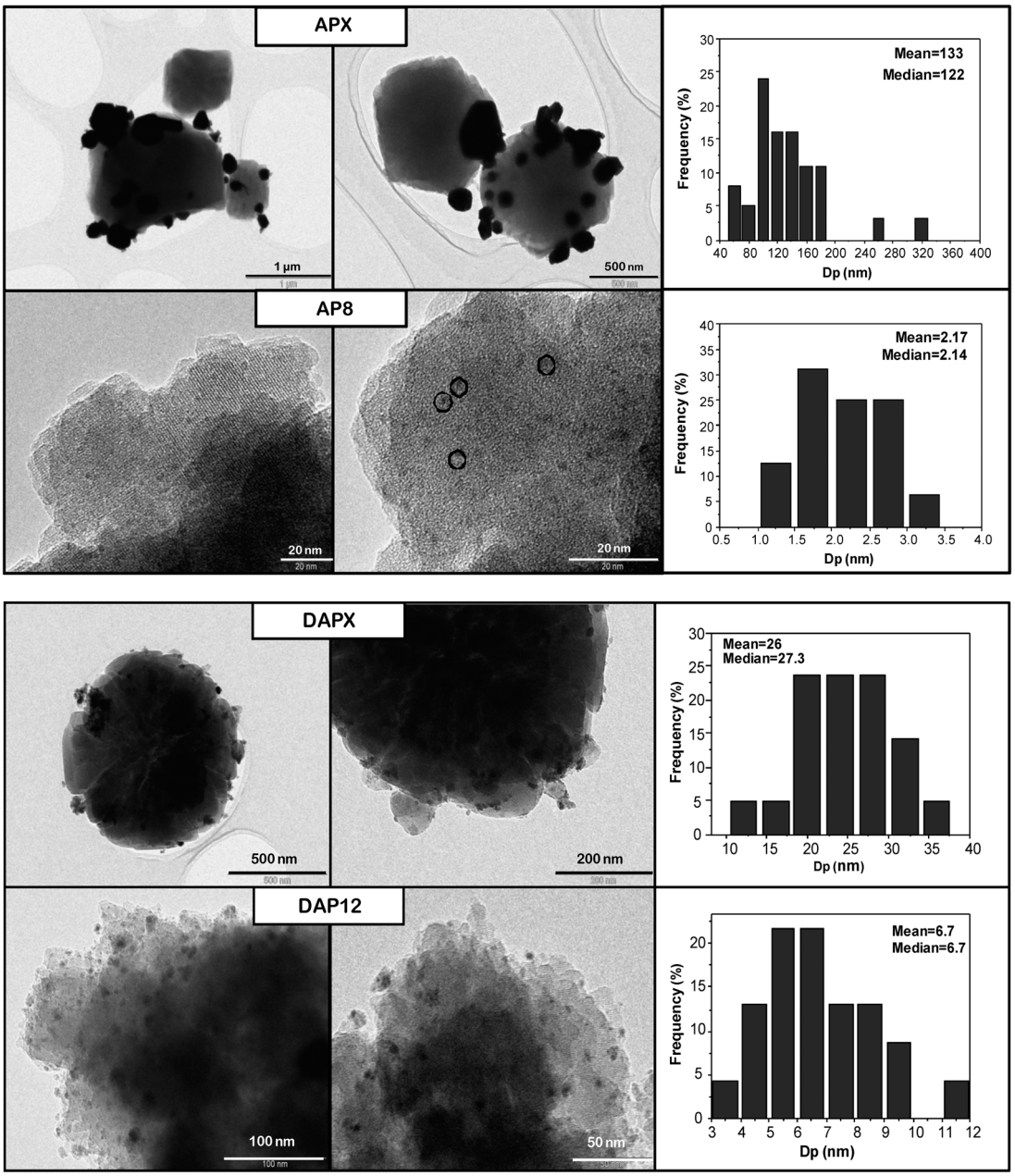

Fig. 4 Representative TEM images and metal particle sizes of AuPd catalyst samples APX, AP8, DAPX and DAP12.

In addition, in some experiments a small amount of benzene is also observed which we consider may be formed by a hydrogenolysis pathway.

Results from these initial studies indicate that these catalysts possess sufficient activity to perform oxidation reactions at much lower temperatures. Subsequent reactions were carried out under a partial pressure of oxygen in a water–methanol solvent mixture (Fig. 6 and Table S1, ESI†). These conditions were adopted as they are used for the direct synthesis of hydrogen peroxide by Edwards *et al.*,[48] however, initially without hydrogen. The use of a water–methanol solvent mixture increases the solubility of the oxygen and hydrogen. In addition, methanol is unable to form peroxides under these conditions.[49] At 2 °C, as expected, the catalytic activity was greatly reduced under these sub-ambient conditions. Comparison of catalysts APX and AP12 illustrates this as the benzaldehyde production rate was found to be 1 ± 0.5 mol h^{-1} $kg_{cat}{}^{-1}$ which is lower than the obtained using TS-1 supports used (*ca.* 5 ± 0.5 mol h^{-1} $kg_{cat}{}^{-1}$) (Table S1, ESI†). Increasing the reaction temperature to 30 °C (Table 4) the rate of disproportionation improved as well as benzaldehyde formation. However, comparison of catalysts APX and AP12 indicates that benzaldehyde selectivity can be improved with secondary porosity. Although, the benzaldehyde production rate was found to be 14 ± 0.5 mol h^{-1} $kg_{cat}{}^{-1}$ over the APX catalyst and this was comparable to the rate over AP8 and DAP12 of 11 ± 0.5 mol h^{-1} $kg_{cat}{}^{-1}$, respectively.

Table 3 Solvent free benzyl alcohol oxidation over various catalysts and the product distribution under low pressure oxygen

Catalyst	Conversion (%)	Selectivity (%)					TOF (h^{-1})	Benzaldehyde production[a] (mol h^{-1} kg_{cat}^{-1})
		Benzene	Toluene	Benzaldehyde	Benzoic acid	Benzyl benzoate		
No catalyst	0.4	5.5	0	93.7	0	0	—	1
TS-1 (XG-REF)	0.4	0	3.8	96.2	0	0	—	1
TS-1 (LG-12%)	0.2	0	0	100	0	0	—	1
AX	0.4	5.9	15.7	76.9	1.4	0	7	1
A12	0.7	0	0	100	0	0	13	2
APX	52.0	0.3	28.2	61.4	9.8	0.3	332	75
AP5	88.9	0.5	37.3	58.2	4.0	0.03	568	122
AP8	88.2	0.6	37.2	60.7	1.3	0.2	564	126
AP12	96.3	0.7	40.0	59.3	0.04	0	615	135
DAPX	50.9	1.7	8.6	85.7	4.1	0	325	103
DAP12	78.4	2.1	2.4	92.3	3.2	0	501	171
PX	19.0	0.5	28.4	66.9	3.7	0.6	121	30
P12	45.3	0.7	23.6	73.7	1.7	0.4	289	79

Conditions: 120 °C, 4 hours, 20 mg of catalyst, 0.0185 mol benzyl alcohol (2 g), P_{O_2}: 1.2 bar (17.4 psi). [a] ±0.5 mol h^{-1} kg_{cat}^{-1}.

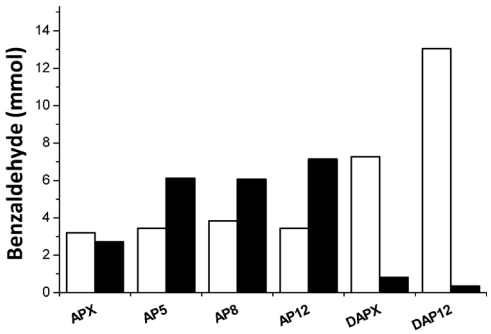

Fig. 5 Moles of benzaldehyde formed through oxidation (□) and disproportionation (■) reactions at 120 °C over AuPd/TS-1 catalysts.

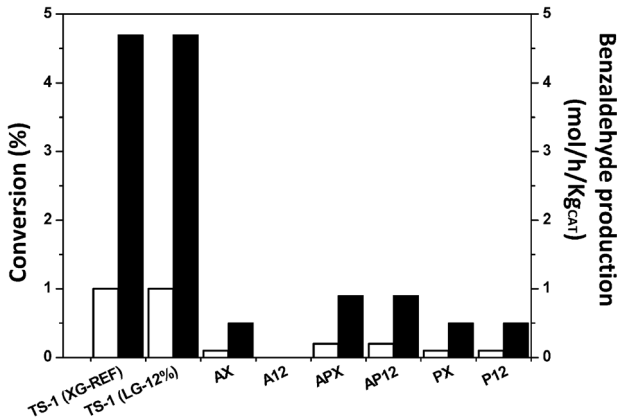

Fig. 6 Benzyl alcohol conversion (□) and benzaldehyde production rate (■) at 2 °C over TS-1 and Au–Pd/TS-1 catalysts. Conditions: 0–2 °C, methanol (5.6 g), water (2.9 g), 2.3 mmol benzyl alcohol (0.25 g), 30 minutes, catalyst (10 mg), 25% O_2/CO_2 (10.4 bar, 150 psi).

To gauge the potential of the catalysts to operate with hydrogen present and improve benzaldehyde yield with an *in situ* generated peroxy species as an oxidant, direct synthesis of H_2O_2 was performed. Fig. 7 and 8 illustrate the production rate of H_2O_2 synthesis at *ca.* 2 and 30 °C respectively and the resulting wt% of peroxide is shown in Tables S2 and S3 (ESI†). The un-modified TS-1 materials were found to be inactive at both temperatures used, as were the Au mono-metallic catalysts. Peroxide production over palladium mono-metallic catalysts PX and P12 indicates that secondary porosity is beneficial at both temperatures tested. The expected synergistic effect of Au–Pd[48] on peroxide production is observable. At *ca.* 2 °C the production rate of H_2O_2 over catalysts APX and AP12 are 34 ± 0.5 and 25 ± 0.5 $mol_{H_2O_2}$ h^{-1} kg_{cat}^{-1} respectively. These values are lower when compared to literature examples; for example over AuPd supported on acid washed carbon or TiO_2 of 160 ± 0.5 and 110 ± 0.5 $mol_{H_2O_2}$ h^{-1} kg_{cat}^{-1} respectively.[50,51] However, at 30 °C (Fig. 8) the peroxide production rate is significantly increased. The rate of reaction is determined by the amount of peroxide remaining in the reaction media at 30 min. The catalyst may bring about an increase in the formation of H_2O as a secondary product, *via* hydrogenation or combustion of the peroxide. We use the rate as a guide to indicate whether a catalyst formulation is likely to support peroxide production and facilitate benzyl alcohol oxidation at a given temperature.

The addition of hydrogen to the benzyl alcohol reaction performed in the autoclave reactor at *ca.* 2 and 30 °C resulted in improvements in the benzaldehyde yield (Tables 5 and 6). Reaction at the lower temperature over mono-metallic gold catalysts (AX and A12) was comparable to reactions without hydrogen, *i.e.* a low rate comparable to data presented in Table 4, *i.e.* <5 mol_{BA} h^{-1} kg_{cat}^{-1}. This, we consider is simply due to the negligible formation of H_2O_2 or hydroperoxy species over these catalysts under these conditions. The presence of Pd in the catalyst as bi-metallic or mono-metallic nano-particles were able to facilitate hydroperoxy formation, as evidenced by the results in Fig. 7. However, the low reaction rate persists at 2 °C over these catalysts even with the *in situ* generation of small amounts of hydroperoxy species.

Increasing the reaction temperature to 30 °C resulted in improvements in the benzaldehyde yield (Table 6). Previously, van der Pol *et al.*[52] have shown that 2-octanol could be oxidised by addition of H_2O_2 at 30 °C over TS-1, although they reported a low total conversion of *ca.* 1.5% after 30 minutes. Therefore, the implication is that Ti centers are active to the formation of

Table 4 Product distribution of benzyl alcohol oxidation in autoclave reactor over various catalysts at 30 °C

Catalyst	Conversion (%)	Selectivity (%)					Benzaldehyde production[a] (mol h^{-1} kg_{cat}^{-1})
		Benzene	Toluene	Benzaldehyde	Benzoic acid	Benzyl benzoate	
TS-1 (XG-REF)	0.1	0	0	100	0	0	1
TS-1 (LG-12%)	0.2	0	0	100	0	0	1
AX	0.1	0	0	100	0	0	1
A12	0.2	0	0	100	0	0	1
APX	4.7	0	31.9	61.2	5.1	1.8	14
AP5	1.6	0	11.1	82.7	6.2	0	6
AP8	2.4	0	3.6	96.4	0	0	11
AP12	1.8	0	8.6	69.1	13.1	9.2	6
DAPX	2.8	0	14.6	80.7	3.1	1.6	11
DAP12	0.2	0	0	100	0	0	1
PX	0.2	0	0	100	0	0	1
P12	0.5	0	0	100	0	0	2

Conditions: 30 °C, methanol (5.6 g), water (2.9 g), 2.3 mmol benzyl alcohol (0.25 g), 30 minutes, catalyst (10 mg), 25% O_2/CO_2 (10.4 bar, 150 psi).
[a] ±0.5 mol h^{-1} kg_{cat}^{-1}.

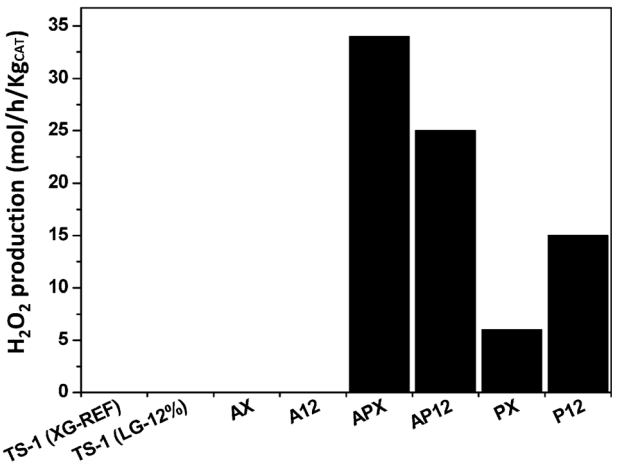

Fig. 7 Production rate of hydrogen peroxide at 2 °C over TS-1 and Au–Pd/TS-1 catalysts. Conditions: 0–2 °C, methanol (5.6 g), water (2.9 g), 30 minutes, catalyst (10 mg), 5% H_2/CO_2 (28.96 bar, 420 psi), 25% O_2/CO_2 (10.4 bar, 150 psi).

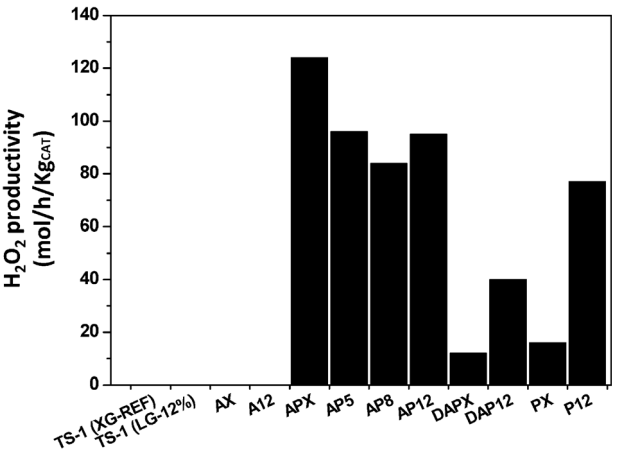

Fig. 8 Production rate of hydrogen peroxide at 30 °C over TS-1 and Au–Pd/TS-1 catalysts. Conditions: 30 °C, methanol (5.6 g), water (2.9 g), 30 minutes, catalyst (10 mg), 5% H_2/CO_2 (28.96 bar, 420 psi), 25% O_2/CO_2 (10.4 bar, 150 psi).

Ti–OOH species at such temperatures. However, below this temperature (20 °C), attempts to oxidize glycerol with H_2O_2 resulted in no reaction,[53] which we also observed for reactions carried out at 2 °C. Diffusion limitations with respect to access of these Ti centers would appear to be a crucial aspect of any potential oxidation reaction. Over the catalysts APX and AP12 the production of benzaldehyde was found to be 29 ± 0.5 and 31 ± 0.5 mol h^{-1} kg_{cat}^{-1} respectively. However, the rate was found to be low with catalyst AP5 and AP8, such that no conclusion can be drawn on the potential benefits of secondary porosity under these conditions. However, we consider that under these conditions the reduced diffusion limitations play a minor role when compared to the presence of metal nano-particles (Au–Pd, Pd). The stability of the peroxide over the larger metal particles of the reference based catalysts is high and potentially this facilitates the high oxidation rate observed (Table 6). The complexity of the reaction pathway is difficult to define with respect to adsorbed metal nano-particles, availability of Ti centers and the stability of the produced peroxy species. However, the high selectivity to benzaldehyde is encouraging with respect to the potential excess of hydrogen peroxide generated during the reaction. Selectivity to the secondary oxidation reaction product benzoic acid was low and the formation of benzyl benzoate low or negligible. Furthermore, no methyl benzoate, a potential condensation product from the reaction of methanol and benzoic acid, was found.

Comparing the AuPd catalysts prepared by DP (DAPX and DAP12), it can be seen that a combination of secondary porosity and smaller metal particle size facilitates both improved benzyl alcohol conversion and benzaldehyde selectivity. The formation of toluene is retarded in the case of using the hierarchical zeolite; potentially due to metal particle size differences compared to catalysts prepared by impregnation, further enhancing the benzaldehyde selectivity. Compared to the APX-12 series the smaller metal particles may play a role in the combustion of H_2O_2 hence the alcohol oxidation rate may be higher in the case of the smaller crystallites but the smaller metal particles being more active decrease the stability of H_2O_2. Thus in the overall objective of oxidising benzyl alcohol a balance must be found to

Table 5 Product distribution of benzyl alcohol oxidation in autoclave reactor over various catalysts at 2 °C with hydrogen and oxygen present

Catalyst	Conversion (%)	Selectivity (%)					Benzaldehyde production[a] (mol h^{-1} kg_{cat}^{-1})	H_2O_2 residual concentration (wt%)
		Benzene	Toluene	Benzaldehyde	Benzoic acid	Benzyl benzoate		
TS-1 (XG-REF)	0.7	0	0	100	0	0	3	0
TS-1 (LG-12%)	1.1	0	0	100	0	0	5	0
AX	0.1	0	0	100	0	0	1	0
A12	0.2	0	0	100	0	0	1	0
APX	0.7	0	0	77.1	22.9	0	3	0.07
AP12	0.7	0	0	63.0	27.0	0	2	0.03
PX	0.5	0	0	100	0	0	2	0.02
P12	1.4	0	0	100	0	0	7	0.05

Conditions: 0–2 °C, methanol (5.6 g), water (2.9 g), 2.3 mmol benzyl alcohol (0.25 g), 30 minutes, catalyst (10 mg), 5% H_2/CO_2 (28.96 bar, 420 psi), 25% O_2/CO_2 (10.4 bar, 150 psi). [a] ±0.5 mol h^{-1} kg_{cat}^{-1}.

Table 6 Product distribution of benzyl alcohol oxidation in autoclave reactor over various catalysts at 30 °C with hydrogen and oxygen present

Catalyst	Conversion (%)	Selectivity (%)					Benzaldehyde production[a] (mol h^{-1} kg_{cat}^{-1})	H_2O_2 residual concentration (wt%)
		Benzene	Toluene	Benzaldehyde	Benzoic acid	Benzyl benzoate		
TS-1 (XG-REF)	0.1	0	0	100	0	0	1	0
TS-1 (LG-12%)	0.2	0	0	100	0	0	1	0
APX	6.6	2.5	4.7	92.8	0	0	29	0.10
AP5	2.0	0	6.2	93.8	0	0	9	0.10
AP8	1.5	0	6.0	94.6	0	0	7	0.11
AP12	7.0	1.4	4.6	92.6	1.5	0	31	0.13
DAPX	2.6	0	14.6	83.6	1.8	0	10	0.02
DAP12	3.8	0	4.4	93.1	0	2.5	17	0.09
PX	2.4	0	3.7	96.3	0	0	11	0.06
P12	3.4	0	13.1	82.8	1.9	2.3	13	0.08

Conditions: 30 °C, methanol (5.6 g), water (2.9 g), 2.3 mmol benzyl alcohol (0.25 g), 30 minutes, catalyst (10 mg), 5% H_2/CO_2 (28.96 bar, 420 psi), 25% O_2/CO_2 (10.4 bar, 150 psi). [a] ±0.5 mol h^{-1} kg_{cat}^{-1}.

introduce greater access to reactants and retain some form of stability of the peroxide species produced *in situ* in order to affect the greatest oxidation potential.

Conclusions

Hierarchical TS-1 materials were synthesised and used as supports for Au, Pd and AuPd nano-particles. These were tested with the oxidation of benzyl alcohol as a model reaction. The use of *in situ* generated H_2O_2 as an oxidant in this reaction would be attractive and the catalysts were evaluated for peroxide production at 2 and 30 °C. At sub-ambient conditions the rate of oxidation was found to be very low, due to a low production rate of H_2O_2. Increasing the reaction temperature to 30 °C improved the peroxide production rate and hence the benzaldehyde production rate. Comparison of reactions at 30 °C in the presence and absence of hydrogen indicated that the formation of peroxide species is highly advantageous with respect to oxidation rates. Benzaldehyde production rates of *ca.* 30 mol h^{-1} kg_{cat}^{-1} could be achieved when the reaction was carried out with H_2 and *ca.* 5 mol h^{-1} kg_{cat}^{-1} with molecular oxygen. The presence of secondary porosity was found to improve the selectivity of benzaldehyde, particularly with the catalysts prepared by deposition precipitation, since the AuPd particle size was lower for catalysts with secondary porosity and led to better metal dispersion. Therefore, the use of highly active zeolitic material with secondary porosity enables this approach to be potentially broadened to a greater number of oxidisable reactants than previously considered.

Acknowledgements

We thank the EPSRC and Al Jouf University (M. A.) for financial support. I. M. thanks Rey Juan Carlos University for fellowship support during the postdoctoral visit to Cardiff University.

References

1 M. Taramasso, G. Perego and B. Notari, *US Pat.*, 4410501, 1983.
2 C. T. Kresge, M. E. Leonowicz, W. J. Roth, J. C. Vartuli and J. S. Beck, *Nature*, 1992, **359**, 710–712.
3 A. Corma, *Chem. Rev.*, 1997, **97**, 2373–2419.
4 M. G. Clerici, *Met. Oxide Catal.*, 2009, **2**, 705–754.
5 G. T. Kokotailo, S. L. Lawton, D. H. Olson and W. M. Meier, *Nature*, 1978, **272**, 437–438.
6 C. C. Freyhardt, M. Tsapatsis, R. F. Lobo, K. J. Balkus, Jr. and M. E. Davis, *Nature*, 1996, **381**, 295–298.
7 J. Jiang, J. Yu and A. Corma, *Angew. Chem., Int. Ed.*, 2010, **49**, 3120–3145.
8 R. Chal, C. Gerardin, M. Bulut and S. van Donk, *ChemCatChem*, 2011, **3**, 67–81.
9 Y. Fang and H. Hu, *Catal. Commun.*, 2007, **8**, 817–820.

10 I. Schmidt, A. Krogh, K. Wienberg, A. Carlsson, M. Brorson and C. J. H. Jacobsen, *Chem. Commun.*, 2000, 2157–2158.
11 Y. Liu, W. Zhang and T. J. Pinnavaia, *Angew. Chem., Int. Ed.*, 2001, **40**, 1255–1258.
12 M. Choi, H. S. Cho, R. Srivastava, C. Venkatesan, D.-H. Choi and R. Ryoo, *Nat. Mater.*, 2006, **5**, 718–723.
13 D. P. Serrano, R. Sanz, P. Pizarro and I. Moreno, *Top. Catal.*, 2010, **53**, 1319–1329.
14 D. Serrano, R. Sanz, P. Pizarro and I. Moreno, *Chem. Commun.*, 2009, 1407–1409.
15 U. Romano, A. Esposito, F. Maspero, C. Neri and M. G. Clerici, *Stud. Surf. Sci. Catal.*, 1990, **55**, 33–41.
16 A. Corma, P. Esteve, A. Martinez and S. Valencia, *J. Catal.*, 1995, **152**, 18–24.
17 M. S. Holm, E. Taarning, K. Egeblad and C. H. Christensen, *Catal. Today*, 2011, **168**, 3–16.
18 F. Maspero and U. Romano, *J. Catal.*, 1994, **146**, 476–482.
19 R. A. Sheldon and J. Dakka, *Erdoel, Erdgas, Kohle*, 1993, **109**, 520–522.
20 C. B. Khouw, C. B. Dartt, J. A. Labinger and M. E. Davis, *J. Catal.*, 1994, **149**, 195–205.
21 H. Mimoun, in *Peroxides (1983)*, John Wiley & Sons, Ltd., 2010, pp. 463–482.
22 M. D. Hughes, Y.-J. Xu, P. Jenkins, P. McMorn, P. Landon, D. I. Enache, A. F. Carley, G. A. Attard, G. J. Hutchings, F. King, E. H. Stitt, P. Johnston, K. Griffin and C. J. Kiely, *Nature*, 2005, **437**, 1132–1135.
23 C. Della Pina, E. Falletta, L. Prati and M. Rossi, *Chem. Soc. Rev.*, 2008, **37**, 2077–2095.
24 T. Hayashi, K. Tanaka and M. Haruta, *J. Catal.*, 1998, **178**, 566–575.
25 Y. A. Kalvachev, T. Hayashi, S. Tsubota and M. Haruta, *J. Catal.*, 1999, **186**, 228–233.
26 B. S. Uphade, T. Akita, T. Nakamura and M. Haruta, *J. Catal.*, 2002, **209**, 331–340.
27 C. Qi, T. Akita, M. Okumura, K. Kuraoka and M. Haruta, *Appl. Catal., A*, 2003, **253**, 75–89.
28 N. Yap, R. P. Andres and W. N. Delgass, *J. Catal.*, 2004, **226**, 156–170.
29 B. Taylor, J. Lauterbach and W. N. Delgass, *Appl. Catal., A*, 2005, **291**, 188–198.
30 A. K. Sinha, S. Seelan, M. Okumura, T. Akita, S. Tsubota and M. Haruta, *J. Phys. Chem. B*, 2005, **109**, 3956–3965.
31 A. Itoh, Y. Kuroda, T. Kitano, Z. Guo, A. Kunai and K. Sasaki, *J. Mol. Catal.*, 1991, **69**, 215–222.
32 G. Li, J. Edwards, A. F. Carley and G. J. Hutchings, *Catal. Commun.*, 2007, **8**, 247–250.
33 S. Ma, G. Li and X. Wang, *Chem. Lett.*, 2006, **35**, 428–429.
34 K. Mori, Y. Miura, S. Shironita and H. Yamashita, *Langmuir*, 2009, **25**, 11180–11187.
35 M. S. Yalfani, S. Contreras, J. Llorca, M. Dominguez, J. E. Sueiras and F. Medina, *Phys. Chem. Chem. Phys.*, 2010, **12**, 14673–14676.
36 S. Okada, S. Ikurumi, T. Kamegawa, K. Mori and H. Yamashita, *J. Phys. Chem. C*, 2012, **116**, 14360–14367.
37 P. Landon, P. J. Collier, A. J. Papworth, C. J. Kiely and G. J. Hutchings, *Chem. Commun.*, 2002, 2058–2059.
38 P. Landon, P. J. Collier, A. F. Carley, D. Chadwick, A. J. Papworth, A. Burrows, C. J. Kiely and G. J. Hutchings, *Phys. Chem. Chem. Phys.*, 2003, **5**, 1917–1923.
39 S. Meenakshisundaram, E. Nowicka, P. J. Miedziak, G. L. Brett, R. L. Jenkins, N. Dimitratos, S. H. Taylor, D. W. Knight, D. Bethell and G. J. Hutchings, *Faraday Discuss.*, 2010, **145**, 341–356.
40 M. A. Uguina, D. P. Serrano, G. Ovejero, R. Van Grieken and M. Camacho, *Appl. Catal., A*, 1995, **124**, 391–408.
41 D. P. Serrano, J. Aguado, J. M. Escola, J. M. Rodríguez and Á. Peral, *Chem. Mater.*, 2006, **18**, 2462–2464.
42 B. Taylor, J. Lauterbach and W. N. Delgass, *Catal. Today*, 2007, **123**, 50–58.
43 G. Li, J. Edwards, A. F. Carley and G. J. Hutchings, *Catal. Today*, 2007, **122**, 361–364.
44 P. Paredes Olivera, E. M. Patrito and H. Sellers, *Surf. Sci.*, 1994, **313**, 25–40.
45 D. I. Enache, D. Barker, J. K. Edwards, S. H. Taylor, D. W. Knight, A. F. Carley and G. J. Hutchings, *Catal. Today*, 2007, **122**, 407–411.
46 S. S. Hladyi, M. K. Starchevsky, Y. A. Pazdersky, M. N. Vargaftik and I. I. Moiseev, *Mendeleev Commun.*, 2002, 45–46.
47 M. Sankar, E. Nowicka, R. Tiruvalam, Q. He, S. H. Taylor, C. J. Kiely, D. Bethell, D. W. Knight and G. J. Hutchings, *Chem.–Eur. J.*, 2011, **17**, 6524–6532.
48 J. K. Edwards, B. E. Solsona, P. Landon, A. F. Carley, A. Herzing, C. J. Kiely and G. J. Hutchings, *J. Catal.*, 2005, **236**, 69–79.
49 M. Piccinini, E. Ntainjua N, J. K. Edwards, A. F. Carley, J. A. Moulijn and G. J. Hutchings, *Phys. Chem. Chem. Phys.*, 2010, **12**, 2488–2492.
50 J. K. Edwards, E. Ntainjua N, A. F. Carley, A. A. Herzing, C. J. Kiely and G. J. Hutchings, *Angew. Chem., Int. Ed.*, 2009, **48**, 8512–8515.
51 J. K. Edwards, B. Solsona, E. Ntainjua N, A. F. Carley, A. A. Herzing, C. J. Kiely and G. J. Hutchings, *Science*, 2009, **323**, 1037–1041.
52 A. J. H. P. van der Pol and J. H. C. van Hooff, *Appl. Catal., A*, 1993, **106**, 97–113.
53 P. McMorn, G. Roberts and G. Hutchings, *Catal. Lett.*, 1999, **63**, 193–197.

